New Class of Rearrangeable Nonblocking Multicast Free-Space Optical Switches

Abdelbaset S. Hamza, Jitender S. Deogun, and Dennis R. Alexander

***Abstract*—In this paper, we propose $N \times N$ rearrangeable nonblocking multicast free-space optical switches. Our design exploits *nonmovable* tri-state switching elements (T-SEs) that support signal splitting and switching simultaneously and seamlessly, and thus, separate splitting stages used in the conventional multicast switches are not needed. It follows that the propagation loss that may be encountered by an optical beam passing through a splitting stage followed by a crossbar (e.g., splitter-and-delivery-based switches) can be avoided in the proposed switch, since the beam passes through only a single stage. The proposed switch exhibits an optimal hardware complexity, as it requires only $N(N+1)/2$ T-SEs. The switch is analyzed and compared to existing optical multicast switches in terms of hardware complexity, power loss, and cost. Comparison results show that the proposed switch provides multicast capability with a lower hardware complexity and a comparable performance. Cost analysis shows that for $N = 4$, the overall cost of the new design is lower than that of existing strictly nonblocking switches, even if the T-SE is 3.5 to 10 times the cost of typical microelectromechanical systems mirrors. In addition, we present a simple routing algorithm that systematically establishes connections over the new switch.**

***Index Terms*—Free space optical; MEMS; Multicast; Optical switching; Switching.**

I. Introduction

Emerging bandwidth-intensive big data applications, such as social media and the Internet of things (IoT), are pushing existing network infrastructures to their limits. For example, International Data Corporation expects that the IoT market will grow from 9.1 billion devices and objects connected to the Internet in 2013 to 28.1 billion by 2020 [1]. This impacts not only the access and data center networks but also the backbone networks. The Industry-Driven Elastic and Adaptive Lambda Infrastructure for Service and Transport Networks (IDEALIST) project [2] estimates that the compound annual growth rate of Internet traffic in backbone networks is 35%. Optical networks have been long seen as a viable solution because of their inherent high bandwidth and data rates. One of the critical optical technologies in optical networks is the optical switch. Different optical switch design aspects must be taken into consideration depending on the type of network (e.g., access, data center, or backbone) and data traffic.

An optical switch can be implemented that is either guided (using waveguides) or in free space [using free space optics (FSO)]. In guided optical switches, technologies such as semiconductor optical amplifiers (SOAs) [3] or array waveguide grating routers (AWGRs) [4] with tunable wavelength converters or tunable lasers can be used to realize fast optical switches with switching times in the range of a few nanoseconds. Switches based on AWGRs or SOAs are usually expensive [5]. On the other hand, FSO switches have low insertion loss and cross talk and simple fabrication, and are less expensive and data rate independent [6]. However, FSO switches are slower than guided switches, and the switching time is in the range of tens of milliseconds.

A common approach for developing FSO switches is to use 2D/3D microelectromechanical systems (MEMS) [6]. MEMS designs use *movable* mirrors to direct beams from inputs to outputs, which may lead to losses due to angular misalignments. Another approach to developing FSO switches is to use electro-optic and liquid crystal materials [6,7], where an electric field is used to configure switching elements (SEs) into either transmissive or reflective states.

Multicast (one-to-many) communication, increasingly becoming a key enabler for many of the emerging applications and services, can be implemented using electronic or optical switches. In electronic switches, optical–electrical–optical (O-E-O) conversion is an essential step. However, multicast in optical communication can be performed more efficiently in the physical layer, utilizing the propagation properties of light. This maintains the data in the optical domain until they reach their destinations, eliminating the need for the O-E-O conversions. Enabling multicast in the physical layer of the optical domain, however, requires the development of efficient *multicast-capable optical switches* [8].

Another important aspect of switch design is its blocking characteristics. A strictly nonblocking (SNB) switch allows an input signal to be directed to any available output, or a set of outputs (if multicast capable), irrespective of the current state of the switch. A rearrangeable nonblocking

Manuscript received February 22, 2016; revised June 7, 2016; accepted June 16, 2016; published July 21, 2016 (Doc. ID 254776).

A. S. Hamza (e-mail: ahamza@cse.unl.edu) and J. S. Deogun are with the Department of Computer Science and Computer Engineering (CSE), University of Nebraska-Lincoln, Lincoln, Nebraska 68588-0115, USA.

A. S. Hamza and D. R. Alexander are with the Department of Electrical and Computer Engineering (ECE), University of Nebraska-Lincoln, Lincoln, Nebraska 68588-0511, USA.

http://dx.doi.org/10.1364/JOCN.8.000569

(RNB) switch allows an input signal to be directed to one or more available outputs; however, rearranging already existing connections may be required. SNB switches have better blocking attributes compared to RNB switches, at the cost of increased hardware complexity. In some realistic cases, however, RNB design is sufficient if the requests are known *a priori* [9]. For example, in wavelength division multiplexing (WDM) or dense WDM backbone networks, the setup of connections is based on the demands of multiple Gbps links, and thus connections can tolerate relatively long setup times involving the rearranging of existing connections to host a new one [10]. Therefore, designing RNB switches is of a practical interest.

Most existing FSO designs are for SNB unicast communication [6], and thus incorporating multicast into these switches requires additional hardware (e.g., splitters), leading to higher hardware complexity. Accordingly, the design of multicast FSO switches with reduced complexity is an interesting yet challenging problem. To this end, we propose a new (to our knowledge) $N \times N$ *RNB multicast FSO* switch using only $N(N+1)/2$ *nonmovable* SEs. Compared to existing multicast optical switches, the new switch is shown to exhibit an optimal hardware complexity, and has a reduced cost. The remainder of the paper is organized as follows. In Section II, we review existing FSO multicast switches. We dedicate Sections III and IV to presenting and analyzing the new RNB multicast switch. Comparative analysis is presented in Section V, followed by conclusions in Section VI.

II. Related Work

In this section, we introduce notation and review existing multicast FSO switches.

A. Notation

An $N \times N$ switch has N input ports, $\mathcal{I} = \{I_1, \ldots, I_N\}$, and N output ports, $\Omega = \{O_1, \ldots, O_N\}$. A connection request between an input port and an ordered set of output port(s) is denoted by $\mathcal{R}_p = \langle I_p, \Omega_p \rangle$, where I_p, $1 \le p \le N$ and Ω_p, $\Omega_p \subseteq \Omega$. A request $\mathcal{R}_p$ is said to be a multicast if $1 < |\Omega_p| < N$, a unicast if $|\Omega_p| = 1$, or a broadcast if $|\Omega_p| = N$ (i.e., $\Omega_p = \Omega$). A set of all requests in an $N \times N$ switch, $\mathcal{R}^{N \times N}$, can be any combination of unicast requests Γ ($1 \le |\Gamma| \le N$) and multicast requests Ψ ($1 \le |\Psi| \le \lfloor N/2 \rfloor$).

B. MEMS-Based FSO Multicast Switches

Several multicast optical switch architectures have been investigated in the literature (e.g., [11–14]). Optical *splitter-and-delivery (SaD)* is a well-known SNB multicast switch [11]. Figure 1(a) shows an $N \times N$ SaD switch where each input beam is initially split into N identical branches using a $1 \times N$ splitter. Corresponding branches from all N splitters are connected to one output port. Thus, any input can be connected to any number of output ports. It is worth noting that a SaD switch does not distinguish between unicast and multicast requests, which results in unnecessary splitting and signal losses. To avoid unnecessary splitting, configurable splitters may be used. This, however, adds to the complexity of the switch design [13].

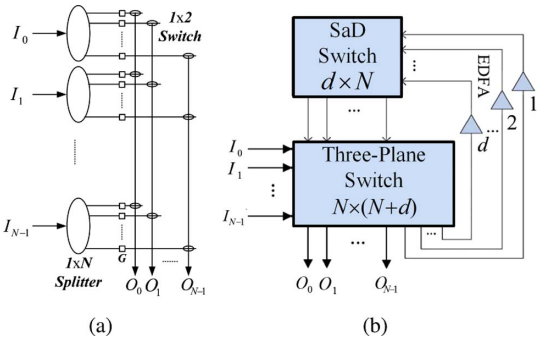

Fig. 1. $N \times N$ switch: (a) SaD [11], (b) SUM-SaD [12]. EDFA, erbium-doped fiber amplifier.

A MEMS-based multicast FSO switch can be implemented using the SaD architecture [11] by replacing the 1×2 switches with MEMS mirrors, and we refer to this switch as *SaD-I*. In Fig. 2(a) we propose a possible realization of a 1×4 FSO splitter. An input signal is split into four beams using a fixed beam-splitting mirror. The total number of components used in a $1 \times N$ splitter is $\Phi = 2^{\lceil \log_2(N) \rceil + 1} - 2$.

SaD-I can be further improved by employing *configurable* splitters (we refer to them as *SaD-II*). Figure 2(b) shows a possible realization of a configurable 1×4 splitter. The total number of components used in a $1 \times N$ configurable splitter is 2Φ. In SaD-II switches, each input beam is divided into a number of beams equal to the cardinality of the output set ($|\Omega_p|$), eliminating unnecessary splitting [13]. It can be seen that SaD-II behaves like a MEMS crossbar and SaD-I in the case of unicast and broadcast, respectively.

A switch that separates unicast and multicast requests (SUM-SaD) is proposed by Zhang and colleagues in [12,14]. The architecture combines a $d \times N$ SaD switch and an

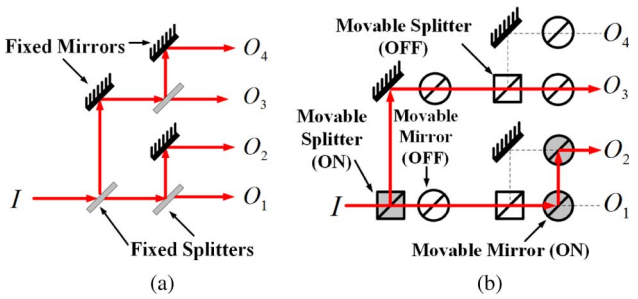

Fig. 2. Possible realization of a 1×4 FSO splitter: (a) conventional, (b) configurable.

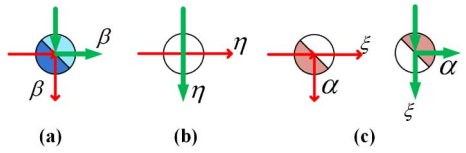

Fig. 3. T-SE: (a) R state, (b) T state, (c) S state.

$N \times (N + d)$ three-plane switch that is basically a 2D MEMS switch [Fig. 1(b)]. To realize an SNB SUM-SaD, the SaD switch must accommodate the maximum number of simultaneous multicast requests that corresponds to half of the input ports, with each multicasting to two output ports (i.e., $d = \lfloor N/2 \rfloor$). Unicast requests are switched by the three-plane switch, and only multicast requests are delivered by the SaD switch. Thus, splitting loss for unicast and multicast is similar to that of SaD-II and SaD-I, respectively.

SaD-based switches are inherently SNB, and thus realizing RNB multicast switches using MEMS mirrors is impractical. This is because MEMS mirrors either pass or reflect the incident beam but cannot split it. Thus, splitting capability needed for multicasting necessitates the use of separate splitters. Each $1 \times N$ splitter generates N copies of the input signal [Fig. 1(a)], and hence, N mirrors are required to connect one of the copies to the corresponding output. This means that an $N \times N$ switch must be used, which is an SNB crossbar, making the design of an RNB in this case meaningless.

In [9], Shen *et al.* propose a MEMS-based triangular switch. However, the proposed architecture and its routing algorithm are suitable only for unicast requests.

C. SNB FSO Multicast Switches Using T-SEs

In [15,16], we propose an SNB multicast FSO crossbar using *nonmoveable* tri-state switching elements (T-SEs). A T-SE can be configured in three states (see Fig. 3): the *reflective* (R), *transmissive* (T), or *splitting* state (S) (half reflective/half transmissive) [15–17].

SE (p,q) denotes a T-SE at the intersection of input port p and output port q $(1 \le p,q \le N)$. The configuration

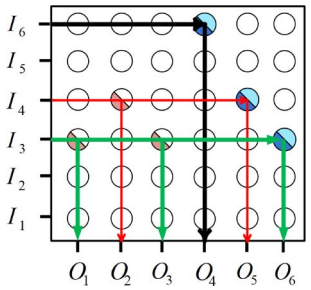

Fig. 4. Multicast in 6×6 crossbar using T-SEs.

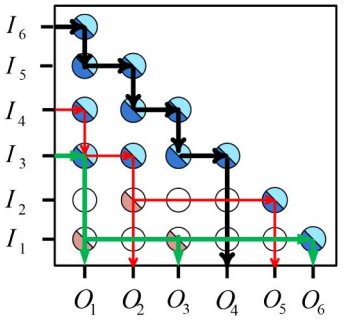

Fig. 5. Multicast in 6×6 proposed switch using T-SEs.

of SE (p,q) is denoted by $\tau(p,q,\chi)$, where $\chi \in \{R,T,S\}$ represents the state of the T-SE. It is assumed that all T-SEs are initially in the T state.

Figure 4 shows a 6×6 crossbar employing T-SEs with one unicast request, $\langle 6,4 \rangle$, and two multicast requests, $\langle 3,\{1,3,6\} \rangle$ and $\langle 4,\{2,5\} \rangle$. Request $\langle 3,\{1,3,6\} \rangle$ is realized by configuring T-SEs as follows: $\tau(3,1,S)$, $\tau(3,3,S)$, and $\tau(3,6,R)$.

III. Proposed RNB Multicast FSO Switch

In this section, we propose a new RNB multicast switch and present a routing algorithm to systematically establish connections over the proposed switch. In the next section, we present and analyze the properties of the proposed switch.

In our design, we aim to use the minimum number of T-SEs to perform RNB multicast switching without impacting the performance of the switch. Therefore, in the proposed switch, a T-SE is placed at the intersection of input port p and output port q only if $p \le q$. This leads to a triangular switch in which a row corresponding to input port p contains $N + 1 - p$ T-SEs, as shown in Fig. 5.

Figure 5 depicts a 6×6 proposed triangular switch with one unicast request, $\langle 6,4 \rangle$, and two multicast requests, $\langle 3,\{1,3,6\} \rangle$ and $\langle 4,\{2,5\} \rangle$. Both T-SE sides reflect light in the R state. A light beam incident to any of the T-SE sides can propagate through or split in the T or S state, respectively. The proposed switch requires only $N(N+1)/2$ T-SEs.

A. Proposed Request-Routing Algorithm

Algorithm 1 is proposed for the configuration (routing) of connections on the proposed multicast switch. In this algorithm, let $\Omega_p = \{O^p_{q,k} | 1 \le q \le N, 1 < k \le |\Omega_p|$ and $\forall\, v,w \in k; O^p_{q,v} < O^p_{q,w}$ if $v < w\}$.

The proposed iterative algorithm involves the elimination process, where $\hat{N}$ denotes the virtual switch size and $\hat{p}$ and $\hat{O}^p_{q,k}$ denote the input and output port indices, respectively.

Algorithm 1 Request Routing

Input: Set of Requests $\mathcal{R}$.
Output: States of the $N(N+1)/2$ T-SEs.

1 $\hat{N} \leftarrow N$
2 **for** *Counter* $= 1 \rightarrow |\mathcal{R}|$ **do**
3 Update list of virtual input and output ports
4 **if** $(\mathcal{R}_p \in \Gamma || (\mathcal{R}_p \in \Psi \,\&\, \&\hat{p} > 1))$ **then**
5 **if** $\hat{O}^p_{q,1} \leq \hat{N} + 1 - \hat{p}$ **then**
6 Configure $\tau(d, \hat{O}^p_{q,1}, R)$ for $d = \hat{p} \rightarrow \hat{N} + 1 - \hat{O}^p_{q,1}$
7 Eliminate SE$(\hat{p}, d)$ for $d = 1 \rightarrow \hat{O}^p_{q,1}$
8 **else**
9 $i \leftarrow \hat{p}$
10 $j \leftarrow \hat{N} + 1 - \hat{p}$
11 **while** $j < \hat{O}^p_{q,1}$ **do**
12 Configure $\tau(i, j, R)$ and $\tau(i-1, j, R)$
13 $i \leftarrow i - 1$
14 $j \leftarrow j + 1$
15 Configure $\tau(i, j, R)$
16 Eliminate SE$(\hat{p}, d)$ for $d = 1 \rightarrow \hat{N} + 1 - \hat{p}$
17 Eliminate SE$(d, \hat{N} + 1 - d)$ for $d = i + 1 \rightarrow \hat{p} - 1$
18 **if** $\mathcal{R}_p \in \Gamma$ **then**
19 Eliminate SE$(d, \hat{O}^p_{q,1})$ for $d = 1 \rightarrow \hat{N} + 1 - \hat{O}^p_{q,1}$
20 $\hat{N} \leftarrow \hat{N} - 1$
21 **else**
22 **for** $d = \hat{O}^p_{q,1} \rightarrow \hat{O}^p_{q,|\Omega_p|-1}$ **do**
23 Configure $\tau(1, d, S)$
24 Eliminate SE(w, d) for $w = 1 \rightarrow \hat{N} + 1 - d$
25 **for** $d = 1 \rightarrow \hat{N} + 1 - \hat{O}^p_{q,|\Omega_p|}$ **do**
26 Configure $\tau(d, \hat{O}^p_{q,|\Omega_p|}, R)$
27 Eliminate SE$(d, \hat{O}^p_{q,|\Omega_p|})$
28 Eliminate SE$(1, d)$ for $d = 1 \rightarrow \hat{O}^p_{q,|\Omega_p|}$
29 $\hat{N} \leftarrow \hat{N} - |\Omega_p|$
30 Route light beams of all requests $\mathcal{R}$.

B. Example

To illustrate the proposed algorithm, we discuss an example that covers different switching scenarios. Figure 6 depicts an 8×8 switch with three unicast and two multicast requests configured using Algorithm 1, namely, $\langle 4, 5\rangle$, $\langle 5, 1\rangle$, $\langle 6, 7\rangle$, $\langle 2, \{2, 6\}\rangle$, and $\langle 8, \{3, 4, 8\}\rangle$. We use T-SEs with solid colors in Figs. 6(a)–6(e). White-, blue-, and yellow-filled circles are used to refer to T-SEs in the T, R, and S states, respectively. Then the final solution is presented using the T-SE symbols shown in Fig. 3.

To configure the switch, we first process the $|\Gamma| = 3$ unicast requests. Requests $\langle 4, 5\rangle$ and $\langle 5, 1\rangle$ [Figs. 6(a) and 6(b), respectively] have $q \leq N + 1 - p$, and hence, there is a T-SE that can directly reflect the light beam from I_p to O_q. When a T-SE is configured in the R state, all T-SEs corresponding to the same column q and higher input ports are also configured in the R state (line 6). This guarantees that the light routed from these input ports reach their destinations through multiple reflections [9]. After each iteration, the row (lines 19–20) and the column (line 7) of the configured T-SEs are crossed and the remaining T-SEs are used to realize a smaller virtual switch.

Figure 6(c) shows the realization of the request $\langle 6, 7\rangle$, where $q > N + 1 - p$. Here, at least three reflections are needed in order to connect I_p to O_q (lines 9–15). After processing the unicast requests, a virtual switch is defined by eliminating the input row (lines 19–20), output column, and any diagonal SEs used in routing the path (lines 16–17).

After processing unicast requests, we process multicast requests in ascending order of the input port indices. Figure 6(d) depicts the realization of the multicast request $\langle 2, \{2, 6\}\rangle$. For a multicast request, first we configure the routing as in the unicast case from the input port to the lowest-index output port in the request (I_2 to O_2 in this example). After the first output port, a series of split operations ending in a reflect operation are configured in the lowest row of the switch (i.e., $\hat{p} = 1$) to route the signal to other output ports (lines 22–29). Similarly, the multicast request $\langle 8, \{3, 4, 8\}\rangle$ is realized [Fig. 6(e)]. The switch with all requests configured is shown in Fig. 6(f).

IV. Properties of the Proposed Switch

In this section, we prove that the proposed switch is RNB and discuss its properties, including hardware complexity, signal path length, and switch reconfigurability.

A. Switch Blocking Characteristics

In the following, we prove Theorem 1 to establish that the proposed triangular switch employing T-SEs is an RNB multicast switch. We start by proving the following lemma that is used in the proof of the theorem. In this lemma, we consider a rectangular switch as shown in Fig. 7. The north and west sides of the switch are used as inputs and are referred to as I^{North}_p and I^{West}_p, respectively, where $1 \leq p \leq M$. The south and east sides are used for outputs, and the corresponding sets of output ports are referred to as $\Omega^S = \{O^{\text{South}}_1, \ldots, O^{\text{South}}_M\}$ and $\Omega^E = \{O^{\text{East}}_1, \ldots, O^{\text{East}}_M\}$, respectively.

Lemma 1. *An $M \times M$ crossbar with $2M$ input and $2M$ output ports shown in Fig. 7 is SNB under the following conditions:*

(1) $1 \leq |\mathcal{R}^{M \times M}| \leq M$,
(2) *a west input I^{West}_p, $1 \leq p \leq M$ can be switched to an arbitrary unused subset of south output ports Ω^{South}_p and/or the corresponding east output port O^{East}_p, and*
(3) *a north input I^{North}_p where $1 \leq p \leq M$ can be switched to an arbitrary unused subset of south output ports $\{O^{\text{South}}_y | p \leq y \leq M\}$ and/or any one of the unused east output ports $\{O^{\text{East}}_z\}$, where $1 \leq z \leq M$.*

Proof. Assume that all of the requests are from west input ports $I^{\text{West}}_1, \ldots, I^{\text{West}}_M$. For each request $\mathcal{R}_p = \langle I^{\text{West}}_p, \Omega_p\rangle$, one of the following cases applies:

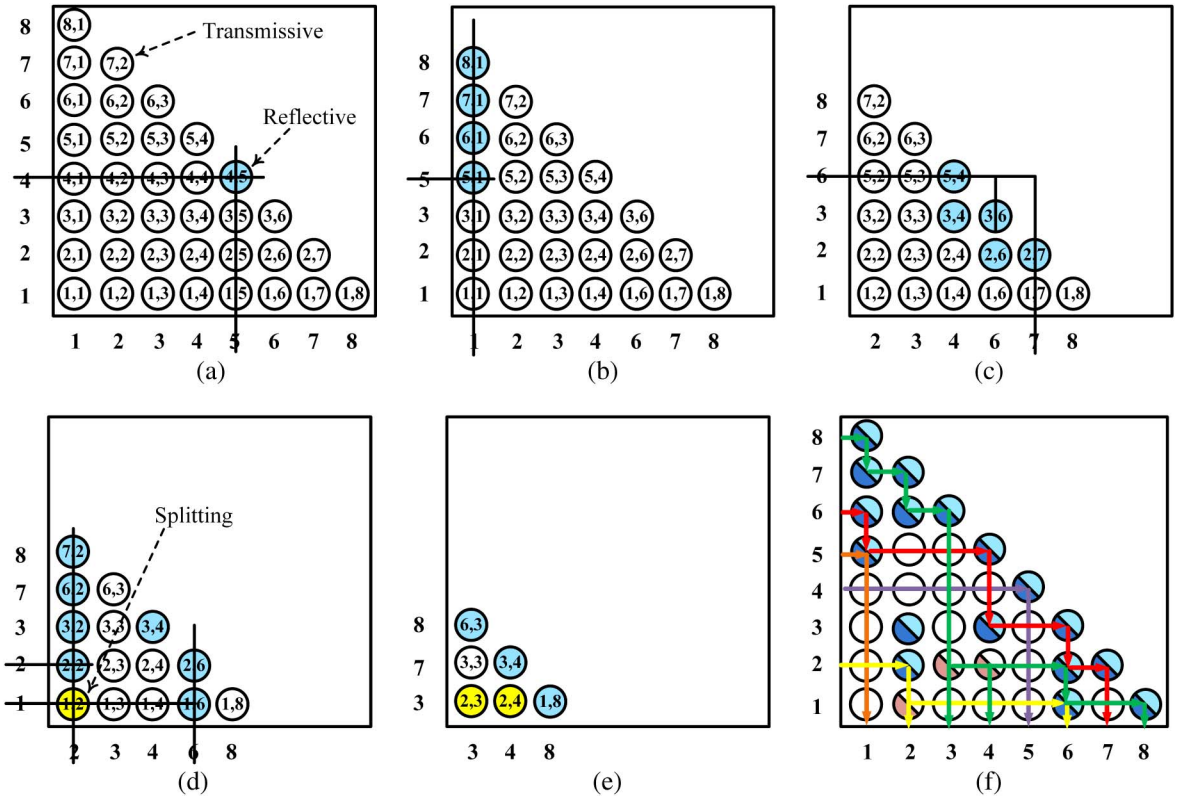

Fig. 6. This figure illustrates the process of configuring the 8×8 proposed switch with three unicast and two multicast requests using Algorithm 1. Black lines indicate the T-SEs that will be eliminated at the end of the current iteration. Each part shows the accumulative result of a request being routed. (a) Unicast request $\langle 4, 5\rangle$, (b) unicast request $\langle 5, 1\rangle$, (c) unicast request $\langle 6, 7\rangle$, (d) multicast request $\langle 2, \{2, 6\}\rangle$, (e) multicast request $\langle 8, \{3, 4, 8\}\rangle$, (f) fully configured switch with all requests.

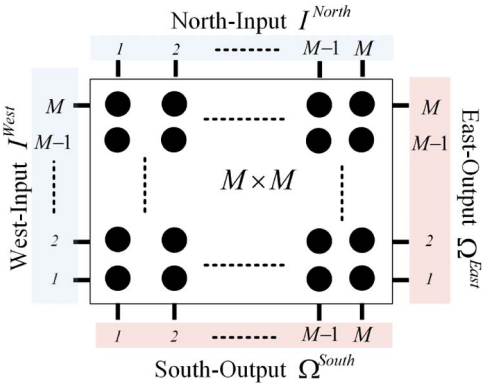

Fig. 7. $M \times M$ rectangular subswitch.

Case 1. $\Omega_p = O_p^{\text{East}}$

All T-SEs are configured in the T state and the light directly propagates toward the corresponding east output port O_p^{East}.

Case 2. $\Omega_p \in \Omega^{\text{South}}$

The T-SEs corresponding to the output ports are configured in the S state, except for the T-SE corresponding to the last output, which is configured in the R state.

Case 3. $\Omega_p \in \Omega^{\text{South}} \cup O_p^{\text{East}}$

All T-SEs corresponding to the output ports in Ω^{South} are configured in the S state, and no T-SE in the row is configured in the R state. This way, part of the signal propagates toward the corresponding east output port O_p^{East}.

For a canceled request by any of the west input ports $I_1^{\text{West}}, \ldots, I_M^{\text{West}}$, there can be a request by one of the north input ports $I_1^{\text{North}}, \ldots, I_M^{\text{North}}$. This also means that all T-SEs in the row corresponding to the canceled request are configured in the T state and can be used by any new request. Hence, a light beam from the north input port of the new request can be directed through its corresponding column until it gets to the row of the canceled request, where splitting is performed.

Therefore, the $M \times M$ crossbar shown in Fig. 7 is SNB under the three aforementioned conditions. □

Theorem 1. *The proposed triangular switch employing T-SEs is an RNB multicast switch.*

Proof. After processing the $|\Gamma|$ unicast requests, we get a triangular switch to process multicast requests. Assume an $N \times N$ triangular switch (see Fig. 8). We want to prove that an $N \times N$ triangular switch used to process $|\Psi|$ multicast requests, where $1 \le |\Psi| \le N/2$, is RNB.

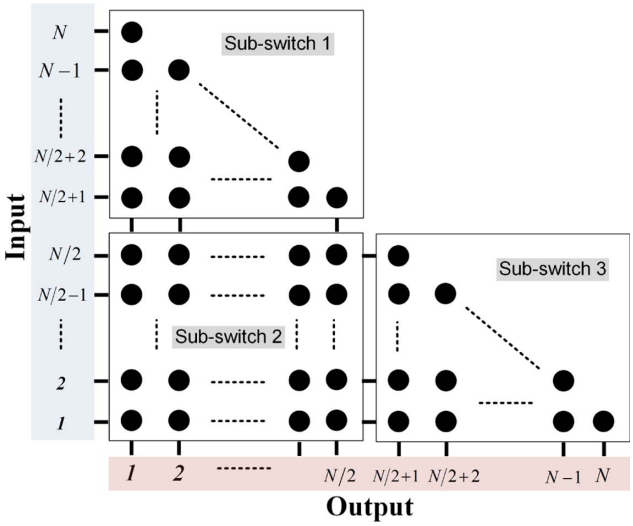

Fig. 8. General structure of an $N \times N$ triangular switch.

We will use induction to prove the theorem. We assume that $N = 2^k$, where $k \in \mathbb{N}^+$. For the basis case, it is clear that all permutations, multicast assignments, and broadcast requests can be realized for a 2×2 switch (i.e., $k = 1$).

Assume by induction that an $N \times N$ triangular switch, where $N = 2^{k-1}$, is RNB. By induction, we wish to prove that an $N \times N$ switch, where $N = 2^k$, is also RNB.

For induction step, an $N \times N$ triangular switch can be divided into three subswitches (see Fig. 8): an $N/2 \times N/2$ rectangular subswitch and two $N/2 \times N/2$ triangular subswitches. The subswitches are numbered from 1 to 3 in counterclockwise order.

Both $N/2 \times N/2$ triangular subswitches are triangular switches of dimensions 2^{k-1}, and thus are RNB by induction hypothesis.

Therefore, for the $N \times N$ triangular switch shown in Fig. 8 to be RNB, we only need to prove that the $N/2 \times N/2$ rectangular subswitch is SNB for processing requests from input ports $I_1, \ldots, I_{N/2}$ and inputs from subswitch 1 (i.e., outputs from subswitch 1).

Using Lemma 1, one can see that subswitch 2 is equivalent to the switch in Fig. 7. Input ports $I_1, \ldots, I_{N/2}$ are equivalent to the west inputs, and inputs from subswitch 1 are equivalent to the north input ports. Moreover, the output ports $O_1, \ldots, O_{N/2}$ are equivalent to the south output ports Ω^{South}, whereas output ports connecting subswitches 2 and 3 are equivalent to the east output ports. Therefore, the $N/2 \times N/2$ rectangular subswitch (i.e., subswitch 2) is SNB, and thus the $N \times N$ triangular switch is RNB. □

B. Hardware Complexity

This is directly proportional to the total number of T-SEs. An $N \times N$ proposed RNB multicast switch requires a total of $N(N+1)/2$ T-SEs. Since the T-SEs of the diagonal are either in the T or R state, the number of T-SEs can be reduced to $N(N-1)/2$ by replacing the N diagonal T-SEs with fixed mirrors.

Theorem 2. *The proposed RNB multicast FSO switch is optimal with respect to hardware complexity as compared to all existing multicast switches.*

Proof. In [18], it is shown that the number of elementary 2×2 switches in an $N \times N$ planar optical RNB unicast switch is at least $N(N-1)/2$. Also, from [9], the lower bound for a 2D *unicast* RNB MEMS switch is $N(N+1)/2$. The proposed RNB multicast FSO switch needs only $N(N-1)/2$ T-SEs (elementary 2×2 switches) and N fixed mirrors. Since the hardware complexity of the proposed switch is equal to the lower bound of a unicast switch, it must be optimal. □

C. Signal Path Length

Several signal paths are possible between a fixed input–output pair (I_p, O_q), $1 \le p, q \le N$, the number of which can be computed using enumerative combinatorics [19]. It may be noted, however, that all paths follow the *taxicab geometry* leading to the following lemma.

Lemma 2. *The length, $\Delta(p,q)$, of any of the possible paths between a fixed pair of input–output ports is expressed in terms of the number of T-SEs traversed by the beam and is given by* $\Delta(p,q) = p + q - 1$ [19].

The path length is constant for a fixed input–output pair (I_p, O_q) and is known *a priori*; however, the numbers of T-SEs in the T and R states are dependent on coexisting connections.

Lemma 3. *It is possible to establish lower and upper bounds for the number of T-SEs in the R state from I_p to O_q, $\mathcal{E}_R(p,q)$, based on the relation between p and q.*

Proof. If $q \le N + 1 - p$, this implies that there is a T-SE at the intersection of row p and column q of the proposed switch. In this case, the input signal can be directed to the output port via a reflection off of that T-SE configured in the R state. Thus, $\mathcal{E}_R(p,q)$ is given by

$$\mathcal{E}_R(p,q) = 1. \tag{1}$$

On the other hand, if $q > N + 1 - p$, then there is not a T-SE at the intersection of row p and column q. At least three reflections are, therefore, needed to direct the input signal to the output port. The lower (upper) bounds for $\mathcal{E}_R(p,q)$ are given by

$$3 \le \mathcal{E}_R(p,q) \le 2\ \min(p-1, q-1) + 1. \tag{2}$$

□

D. Total Number of Splitting Operations

The performance of the proposed switch depends on the number of splitting operations given by the following Lemmas.

Lemma 4. *In multicast, the minimum and maximum number of T-SEs configured in the S state are similar to those of the SNB switch* [15] *and are equal to 1 and* $N-1$, *respectively.*

Proof. This directly follows from the minimum (of 2) and maximum (of N) cardinalities of outputs. □

Lemma 5. *For all requests at a given time, the total number of T-SEs configured in the S state is given by* $N_\Psi - |\Psi|$, *where* $2 \le N_\Psi \le N$ *is the number of output ports in all multicast requests at a certain point in time* $N_\Psi = \Sigma_{w=1}^{|\Psi|}\Omega_w, \forall\ \mathcal{R}_p \in \Psi$, *and* $|\Psi|$ *is the total number of multicast requests.* □

Proof. For each multicast request $\langle I_p, \Omega_p \rangle$, using Algorithm 1, all T-SEs in the first row and columns corresponding to output ports in Ω_p are configured in the S state except for the last output port in Ω_p, which is configured in the R state. Therefore, the total number of T-SEs in the R state out of N_Ψ is equal to the total number of multicast requests $|\Psi|$. □

E. Signal Power Loss

An optical signal in a multicast switch undergoes insertion/coupling and splitting losses as it propagates from input to output ports. Insertion/coupling loss is mainly due to the Gaussian beam divergence experienced by any light beam propagating in free space [20], and thus depends on the architecture of the switch. Extensive analysis and studies have been performed to characterize the insertion/coupling loss in a 2D MEMS crossbar. Insertion/coupling loss in the proposed design follows the analysis used for MEMS switches [20], but with the following two differences:

(1) In MEMS-based multicast switches, a beam must propagate through a splitting stage before being switched by a crossbar. On the other hand, an optical beam propagates only through a single stage in the proposed triangular switch, which may lead to a shorter total propagation distance, and thus lower insertion loss.

(2) Mechanical motion of the mirrors in MEMS switches results in angular misalignment leading to inefficient coupling. Our proposed design employs only *nonmovable* parts, and hence is free of such losses.

Splitting losses are the losses encountered by the light beam due to the splitting required for multicasting. Let β and η be the reflection and transmission efficiencies of T-SE in the R and T states, respectively. We denote the percentage of the power reflected by a T-SE in the S state as α, and the transmitted power of the beam is ζ (Fig. 3). In the proposed switch, splitting losses depend on the cardinality of the output set $|\Omega_p|$, and thus we have two different cases.

Case 1: Unicast ($|\Omega_p| = 1$). The power loss is due to the reflection and transmission losses of the T-SEs configured, respectively, in the R and T states along the path, and thus depends on the number of T-SEs configured in the R state [i.e., $\mathcal{E}_R(p,q)$]. From Lemma 2, the length of a path $\Delta(p,q)$ is known. Given $\mathcal{E}_R(p,q)$, the number of T-SEs configured in the T state is $\Delta(p,q) - \mathcal{E}_R(p,q)$. Since β and η are the reflection and transmission efficiencies of T-SE in the R and T states, respectively, the power penalty in a unicast request, $\mathrm{L_{UC}}(p,q_1)$, can be expressed as follows:

$$\mathrm{L_{UC}}(p,q_1) = 10\log_{10}[\beta^{\mathcal{E}_R(p,q)} \cdot \eta^{\Delta(p,q)-\mathcal{E}_R(p,q)}]. \tag{3}$$

For $q \le N+1-p$, $\mathcal{E}_R(p,q) = 1$ (according to Lemma 3), and thus the power loss is given by

$$\mathrm{L_{UC}}(p,q_1) = 10\log_{10}[\beta \cdot \eta^{\Delta(p,q)-1}], \tag{4}$$

$$\mathrm{L_{MC}}(I_p, O^p_{q,k}) = 10\log_{10}((\sigma\cdot\alpha + (1-\sigma)\cdot\beta) \cdot \beta^{\mathcal{E}_R(p,q)} \cdot \eta^{\Delta(p,q)-k-\mathcal{E}_R(p,q)} \cdot \zeta^{k-1})\ \mathrm{dB}, \tag{5}$$

$$\mathrm{L_{MC}}(I_p, O^p_{q,k}) = 10\log_{10}((\sigma\cdot\alpha + (1-\sigma)\cdot\beta) \cdot \eta^{N-p+q-k} \cdot \zeta^{k-1})\ \mathrm{dB}. \tag{6}$$

Case 2: Multicast ($1 < |\Omega_p| < N$). Power loss at an output port O_q that is part of a multicast output set, Ω_p is due to reflection and transmission losses of the T-SEs in the path configured in the R, T, and S states.

Depending on the position, k, of the output port O_q in the output set Ω_p, we can define how many splitting processes the signal has to go through. For example, the input signal experiences $k-1$ splits before it reaches the kth output port in Ω_p. Therefore, the power loss due to these splits can be calculated as $\log_{10}(\zeta^{k-1})$.

Moreover, all outputs in Ω_p are reached via a reflection off of a T-SE configured in the S state, except for the last output port, which is reached using a reflection off of a T-SE in the R state. Therefore, for all signals we reduce the power by $\log_{10}(\alpha)$, except for the last output port—we reduce its power by $\log_{10}(\beta)$.

Since we know the path length, $\Delta(p,q)$, from Lemma 2, this means that the remaining $\Delta(p,q) - k$ T-SEs in the path can be in either the T or R state depending on the route allocated using Algorithm 1. Given $\mathcal{E}_R(p,q)$, we can use Eq. (6) to express splitting power loss in the case of multicast $\mathrm{L_{MC}}(p, O^p_{q,k})$, where $\sigma = 1$ for $1 \le k < |\Omega_p|$ and $\sigma = 0$ for $k = |\Omega_p|$, to choose from α and β depending on k.

Below, we prove Theorem 3 to show that the splitting loss analysis of the proposed $N \times N$ RNB switch when $\eta = \beta$ is similar to that of the $N \times N$ SNB switch presented in [15].

Theorem 3. *Splitting loss at output ports in the proposed RNB switch are similar to that of an SNB switch* [15] *if* $\eta = \beta$.

Proof. The path length of the connections from I_p to O_q (as a unicast request or part of a multicast request) is fixed. Similarly, the number of splitting operations for $\mathcal{R}_p$ is fixed, and thus the remaining T-SEs are either in the T or in the R state. Since both T and R states have the same power losses, the overall loss is similar to that of our SNB switch [15]. □

Based on Theorem 3, we can use the power loss equations in [15] to calculate the splitting power loss in the proposed switch. Equation (3) for the power penalty in a unicast request becomes

$$L_{UC}(p, q_1) = 10\log_{10}(\eta^{\Delta(p,q)}) = 10\log_{10}(\beta^{\Delta(p,q)}). \quad (7)$$

Similarly, Eq. (5) for the power penalty of multicast requests can be expressed by Eq. (6).

F. Switching Delay

The switching latency depends on the switching speed and the properties of the material used to realize T-SEs. The switching latency of a $1'' \times 1''$ switchable mirror (SM)-based e-TransFlector tuned for the IR spectrum is in the range of 1–10 ms at room temperature (22 °C). The dimensions of the T-SEs in the proposed switch are expected to be much smaller than $1'' \times 1''$. Since the switching latency is proportional to the surface area of the SM, the switching delay can be reduced. Moreover, as the technology of the materials used to realize T-SEs improves, more responsive T-SEs can be developed, and thus faster switches can be realized.

G. Switch Reconfigurability

In Fig. 4, an $N \times N$ SNB crossbar [15,16] requires a square substrate with N^2 T-SEs. On the other hand, two of the proposed $N \times N$ RNB triangular switches would require a triangular substrate with $2 \times (N(N+1)/2) = N(N-1)$ T-SEs. However, as discussed earlier, the diagonal T-SEs in the proposed switch are either in the T or R state, and thus diagonal T-SEs can be replaced with fixed mirrors, or can be configured permanently in the R state. This way, two of the proposed $N \times N$ RNB triangular switches can share the diagonal T-SEs, and hence both switches can be accommodated on a single square substrate with N^2 T-SEs, as shown in Fig. 9.

It should be noted that we can obtain a very flexible switch using the setup in Fig. 9. This switch can operate as two $N \times N$ RNB switches or a single $N \times N$ SNB switch for I^{West}–Ω^{South} or I^{North}–Ω^{East}. Moreover, the switch in Fig. 9 can also operate as a $2N \times 2N$ switch (see Fig. 7) under the constraints outlined in Lemma 1.

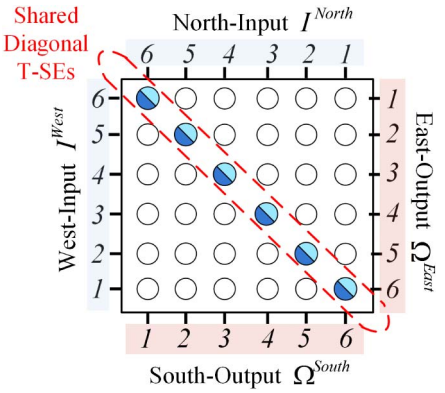

Fig. 9. Two 6×6 RNB switches on a single square substrate.

V. Comparative Analysis

2D FSO switches are generally of low scalability due to the Gaussian beam propagation loss, which becomes the dominant source of losses at a high port count [21]. In this section, we present a comparative analysis of the proposed switch with respect to hardware complexity, power splitting, and cost for $N = 8$ (i.e., 8×8 switches).

A. Hardware Complexity Comparison

We decompose all switches into five basic SEs, namely, fixed and movable mirrors, fixed and movable splitting mirrors, and T-SEs. Table I summarizes the hardware complexity of the architectures under consideration. Figure 10 depicts the hardware complexity for $N = 8$.

In SaD-I, a unicast request must undergo $1 \times N$ splitting. Therefore, no extra hardware is needed to separate unicast requests. SaD-II is similar to SaD-I except that configurable splitters are used to separate unicast and multicast requests, and to split the input beam to the exact size of the output set. However, this comes at the expense of additional hardware and control complexity. SUM-SaD separates unicast and multicast connections and has lower hardware complexity compared to that of SaD-II. Although

TABLE I
Summary of Switching Hardware Complexity of Different Architectures $\Phi = (2^{([\log_2(N)]+1)} - 2)$

	Movable Mirror	Fixed Mirror	Movable Splitter	Fixed Splitter	T-SE
SaD-I	N^2	$N\Phi/2$	—	$N\Phi/2$	—
SaD-II	$N^2 + N\Phi$	$N\Phi/2$	$N\Phi/2$	—	—
SUM-SaD	$2N^2 + N$	$N\Phi/4$	—	$N\Phi/4$	—
Crossbar (T-SE)	—	—	—	—	N^2
Proposed	—	N	—	—	$\frac{N(N-1)}{2}$

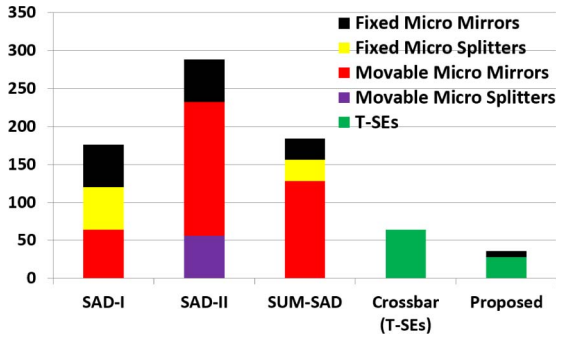

Fig. 10. Hardware complexity for 8×8 switches.

comparable to SaD-I with respect to hardware complexity, SUM-SaD uses more movable SEs.

Similar to SaD-II, an SNB crossbar using T-SEs and the proposed switch can separate unicast and multicast requests, and can also split a beam into a number of beams equal to the size of the output set. A crossbar requires N^2 T-SEs, whereas, the proposed RNB switch requires only $N(N-1)/2$ T-SEs and N fixed mirrors. For $N = 8$, the proposed switch demonstrates 87.5% and 43.8% savings in total number of SEs as compared to SaD-II and the crossbar with T-SEs, respectively.

B. Comparison of Splitting Losses

In the previous section, we showed that the proposed switch can achieve up to an 87% reduction in hardware complexity compared to that of existing switches. In this section, we show that the hardware complexity improvement achieved does not sacrifice the power splitting and scalability properties of the switch. To this end, we discuss the power penalties for the five architectures of size 8×8 by computing the losses at eight output ports for all 255 combinations of output set sizes. Since the loss in the proposed switch depends on the input port, losses for the first (best case) and eighth (worst case) are presented.

In the case of SaD-I, signal power loss is independent of output set size $|\Omega_p|$, as N-way splitting is enforced, and is given by

$$L_{\text{SaDI}} = 10\log_{10}(0.99) + 10\log_{10}(1/N)\ \text{dB}. \tag{8}$$

For SaD-II, the unnecessary splitting of SaD-I is avoided, and thus splitting loss is dependent on $|\Omega_p|$ and is given by

$$L_{\text{SaDII}} = 10\log_{10}(0.99) + 10\log_{10}(1/|\Omega_p|)\ \text{dB}. \tag{9}$$

We use the commercial specifications reported by KentOptronics [22] for the tri-state material e-TransFlector, which can be tuned to operate in the IR spectrum range used by existing optical communication networks. For example, in [23], Hamedazimi *et al.* demonstrated a proof of concept for an FSO communication link for data center communication using the e-TransFlector material tuned for the IR spectrum. Accordingly, we set both the reflectance in the R state (β) and transmittance in the T state (η) to 87%, whereas for the S state, both the transmittance (ζ) and reflectance (α) are set to 43%. We assume that the optical efficiency of all fixed/movable mirrors and splitters are 99% and 49%, respectively [24].

In the power loss study, we use the term *proposed* to refer to both SNB and RNB T-SE based switches. Figures 11(a)–11(c) depict the average minimum, average, and average maximum splitting power loss of the five switch architectures under consideration at different sizes of output sets.

SaD-II and SUM-SaD can switch unicast connections separately without incurring any additional losses, and thus SaD-II and SUM-SaD have the same performance,

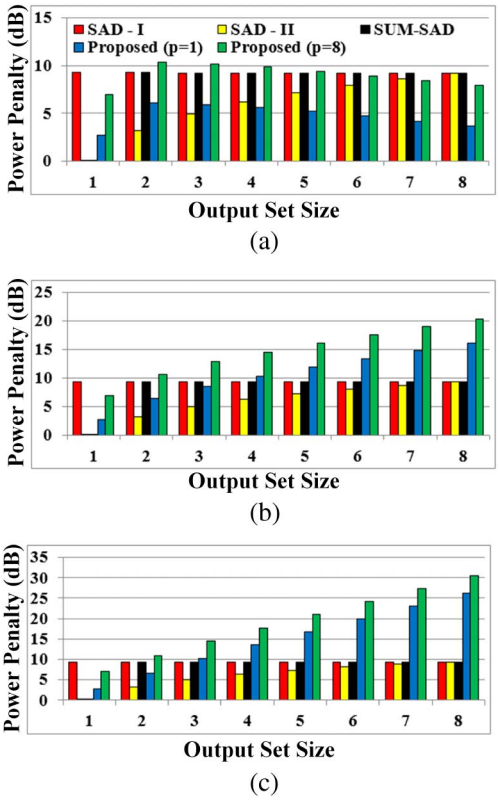

Fig. 11. Splitting power penalty in an 8×8 switch [15] with $\alpha = \zeta = 43\%$ and $\eta = \beta = 87\%$. (a) Minimum. (b) Average. (c) Maximum.

which outperforms other architectures in the case of unicast. On the other hand, unicast requests switched using SaD-I are penalized ≈9.3 dB, as SaD-I enforces full power splitting even for unicast connections. The proposed architecture does not enforce splitting for unicast connections; however, there are additional losses of 4.53 and 7 dB for input ports 1 and 8, respectively. This is due to the propagation of the beam through the nonmoveable T-SEs configured in the T state along its path, which adds additional loss due to the imperfection of the material.

In the case of multicast (i.e., starting from an output set size of two), it can be observed that as the size of the output set increases, so do the average and average maximum power penalties in all architectures except for the SaD-I and SUM-SaD; they have a fixed power loss (≈9.3 dB). This is because SaD-I and SUM-SaD perform fixed full splitting for all input signals regardless of the size of the output set. The proposed switch outperforms both SaD-I and SUM-SaD up to an output size of two, whereas its performance is comparable to the other architectures up to an output set size of four, after which the power loss increases.

Splitting power loss depends on the number of combinations at different sizes of output sets. This number increases starting from an output set size of one (i.e., eight possible combinations of unicast) to four (i.e., 70 possible combinations), and then decreases to become one possible combination of broadcast. Regardless of the decrease in the

number of combinations starting from an output set size of four, the average maximum loss experiences a monotonic increase as the aggregated maximum loss becomes dominant, whereas the average minimum loss decreases as the size of the output set increases.

High power losses can cause the signal power to fall below the sensitivity of the optical receiver, and thus amplification at the input ports may be needed. Moreover, power loss at an output port can vary depending on the configuration of the switch. For example, in the case of an output set size of eight, the variation between the minimum and maximum splitting loss in the proposed switch is 25 dB (see Fig. 11). Therefore, variable optical attenuators (VOAs) must be used at the output ports to equalize the impact of the insertion loss such that the power of the received signal falls within the dynamic range of the optical receiver [21].

It should be noted that MEMS-based switches show relatively lower splitting power losses and do not demonstrate differences between minimum and maximum splitting power loss at the output ports as compared to the proposed switch. This is because we only consider the splitting losses in our analysis. MEMS-based switches, however, incur additional Gaussian beam loss due to the propagation of the beam in the separate splitting stage, and loss due to the angular misalignment of the micromirrors [20,25] which can become significant if the light beam experiences multiple reflections, such as in $1 \times N$ beam splitters [9,26]. Therefore, MEMS-based switches still need preamplifiers, e.g., SUM-SaD [see Fig. 1(b)], and VOAs due to the nonsplitting losses encountered by the signal.

Table II summarizes the number of amplifiers and VOAs required by the switches investigated. The proposed switch, SaD-I, SaD-II, and the T-SE-based crossbar need N amplifiers and N VOAs, whereas the SUM-SaD switch requires N VOAs and only $N/2$ amplifiers. This is because only $N/2$ of the inputs are propagating through the splitting stage, as shown in Fig. 1(b).

Gaussian beam propagation loss is considered the main limiting factor for realizing FSO switches with high scalability. However, other factors, such as material imperfection of T-SE and signal splitting properties, can also limit the scalability of the proposed switch.

The technology of the material used to realize T-SEs is still in its infancy. We use modest values for the material transmittance and reflection efficiencies (i.e., $\eta = \beta = 87\%$ and $\alpha = \zeta = 43\%$ for a 50/50 reflection/transmission splitting ratio). However, as the quality of the material continues to improve, so will the performance of the proposed switch.

TABLE II
NUMBER OF AMPLIFIERS AND VOAS

	Amplifiers	VOAs
SaD-I	N	N
SaD-II	N	N
SUM-SaD	$N/2$	N
Crossbar (T-SEs)	N	N
Proposed	N	N

To understand the impact of the quality of the material used on the performance of the proposed switch, we calculate splitting power loss for the proposed switch assuming improved T-SE efficiencies. We assume that $\eta = \beta = 99\%$ instead of 87%. For the splitting state, we set $\alpha = \zeta = 49\%$ instead of 43%. To measure the improvement in the performance of the proposed switch due to the improved material quality, we consider the worst request scenario, that is, a broadcast request from the eighth input port. We notice an overall reduction in the splitting power penalty for the proposed switch based on the improved parameters. For example, a reduction in the power penalty of 8.5 dB (equivalent to an improvement of 28%) in the case of broadcast from the eighth input port is achieved.

Another factor that limits the scalability of the proposed switch is the *cascaded* splitting nature of the signal power along the way from the input to the outputs. This splitting behavior results in higher power loss and unequal signal power at the output ports. For example, to multicast a signal to four outputs, using a SaD switch will result in 1/4 of the input power at each of the four outputs compared to 1/2, 1/4, 1/8, and 1/8 of the input power in the case of the proposed switch. One way to alleviate this incremental power loss is to change the splitting ratio of the T-SE such that a small fraction of the input signal (e.g., 10%) is tapped at each output port and the remaining 90% of the power is forwarded to the subsequent output ports.

We evaluate the impact of changing the T-SE splitting ratio by calculating the splitting power penalty for the proposed switch assuming a 10/90 splitting reflection/transmission ratio while maintaining $\eta = \beta = 87\%$. Changing the splitting ratio leads to an improvement in the performance of the proposed switch and a reduction of 13.5 dB in the power penalty in the case of broadcast from the eighth input port. This is equivalent to an improvement of 44.3%.

It is possible to further improve the overall performance of the proposed switch by improving the quality of the material used and also changing the T-SE splitting ratio. Figures 12(a)–12(c) depict the average minimum, average, and average maximum splitting power loss at different sizes of output sets assuming improved T-SE quality (i.e., $\eta = \beta = 90\%$) while a splitting ratio of 10/90 is maintained. A significant decrease in the power penalty can be observed. In the case of broadcast from the eighth input, the maximum splitting power penalty is 13 dB, which is less than that in Fig. 11 by 17.44 dB, indicating an improvement of 57.2%.

C. Cost Analysis

From the discussion above, the total cost ($C_{\text{tot}}^{\text{arch}}$) of a switch architecture arch depends on the costs of the VOAs ($C_{\text{VOA}}^{\text{arch}}$), amplifiers ($C_{\text{amp}}^{\text{arch}}$), and SEs ($C_{sw}^{\text{arch}}$) used, and is given by

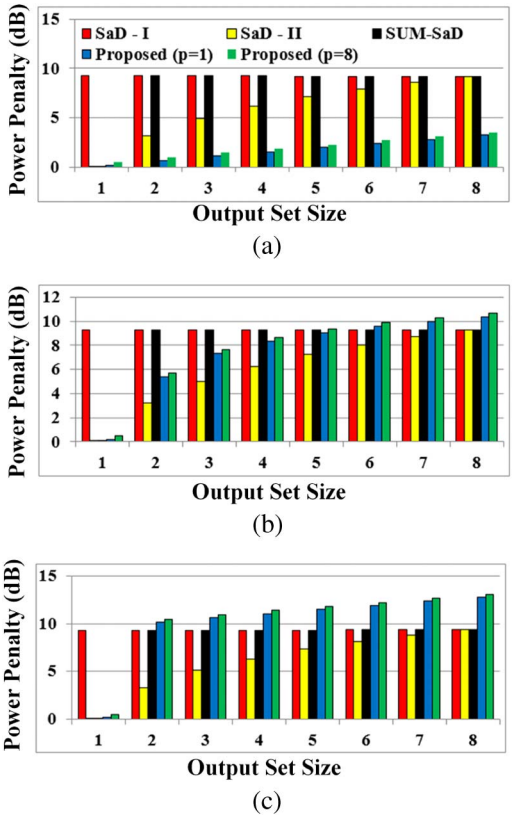

Fig. 12. Splitting power penalty in an 8 × 8 switch with $\alpha = 10\%$, $\zeta = 90\%$, and $\eta = \beta = 99\%$. (a) Minimum, (b) average, (c) maximum.

$$C_{\text{tot}}^{\text{arch}} = C_{\text{VOA}}^{\text{arch}} + C_{\text{amp}}^{\text{arch}} + C_{\text{sw}}^{\text{arch}}, \tag{10}$$

where arch can be SaD-I, SaD-II, SUM-SaD, or the proposed switch. $C_{\text{VOA}}^{\text{arch}}$ and $C_{\text{amp}}^{\text{arch}}$ depend on the number of VOAs ($N_{\text{VOA}}^{\text{arch}}$) and amplifiers ($N_{\text{amp}}^{\text{arch}}$) used, respectively.

From Table II, SaD-I, SaD-II, and the proposed switch architectures employ N VOAs at the output ports and N amplifiers at the input ports. However, SUM-SaD switch architecture requires N VOAs and only $N/2$ amplifiers. Therefore, SUM-SaD architecture has a cost advantage over SaD-I, SaD-II, and the proposed architecture with respect to C_{amp}.

We can expand $C_{\text{sw}}^{\text{arch}}$ further and express it as a function of the cost of a fixed (mirror/splitter) component C_f, a movable (mirror/splitter) component C_m, and a T-SE C_{tse}. Given the cost of each component, we can calculate $C_{\text{sw}}^{\text{arch}}$ as follows:

$$C_{\text{sw}}^{\text{arch}} = N_f^{\text{arch}} \cdot C_f + N_m^{\text{arch}} \cdot C_m + N_{\text{tse}}^{\text{arch}} \cdot C_{\text{tse}}, \tag{11}$$

where N_f^{arch}, N_m^{arch}, and $N_{\text{tse}}^{\text{arch}}$ are the numbers of fixed, moveable, and T-SE switching elements used in the switch arch, respectively, and can be obtained from Table I.

We use a relative cost model to quantify and compare the cost of the proposed switch. We use the cost of the fixed elements, C_f, as reference, since the cost of these components is relatively stable compared to the other two types.

Let $\rho = C_m/C_f$ and $\mu = C_{\text{tse}}/C_f$. To evaluate the cost-effectiveness of the proposed switch as compared to SaD-I, we use the total number of fixed and movable components in Table I to setup the inequality

$$N^2 C_m + N\Phi C_f > \frac{N(N-1)}{2} C_{\text{tse}} + NC_f. \tag{12}$$

From Eq. (12), it is easy to see that the proposed switch has a smaller overall cost compared to that of SaD-I if

$$\rho_{\text{SaD-I}} > \frac{(N-1)\mu + 2 - 2\Phi}{2N}. \tag{13}$$

Similarly, we can compute a lower bound on the value of ρ for the SaD-II and SUM-SaD as follows:

$$\rho_{\text{SaD-II}} > \frac{(N-1)\mu + 2 - \Phi}{2N + 3\Phi}, \tag{14}$$

$$\rho_{\text{SUM-SaD}} > \frac{(N-1)\mu + 2 - \Phi}{4N + 2}. \tag{15}$$

Figure 13 plots the ratio ρ/μ to provide insight into the relationship between the cost of a T-SE and that of a movable component. Given the cost of various hardware components, one can use Fig. 13 to determine the cost-effectiveness of the proposed design with respect to SEs as compared to SaD-based switches at different port sizes ($N = 4$, 8, and 16). The function $1/\mu$ (i.e., $\rho = 1$) corresponds to the case in which $C_m = C_f$. Obviously, the cost of a moveable element $C_m > C_f$, and thus the shaded area below the curve $1/\mu$ is

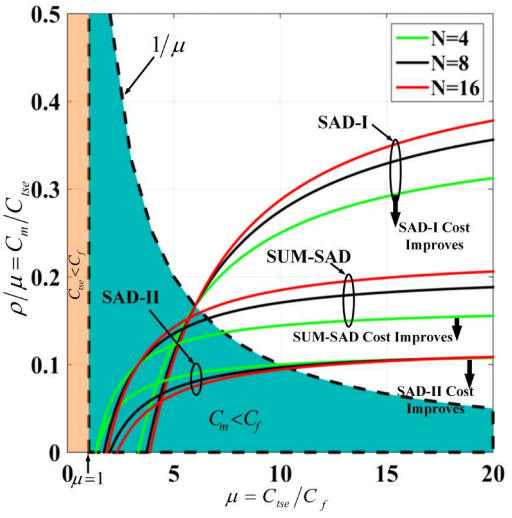

Fig. 13. Comparative cost analysis for the proposed switch. The curves represent the relative cost effectiveness of the proposed switch compared to the existing SaD switches with respect to switching elements. Shaded regions are invalid design regions. The white region above (below) a curve indicates that the proposed switch is more (less) cost effective compared to the corresponding SaD switch for a specific number of ports N.

considered as an *invalid design region*. It is not expected that C_{tse} will be less than C_f. Therefore, we have also excluded the area corresponding to $\mu < 1$. The white region above (below) a curve indicates that the proposed switch is more (less) cost-effective compared to the corresponding SaD switch for a specific number of ports N. For example, for $N = 4$, even if the cost of a T-SE is 15 times the cost of fixed components (i.e., $\mu = 15$), the proposed switch will be more cost-effective compared to the SaD-I, SUM-SaD, and SaD-II, even when C_{tse} is 3.5, 6.7, or 10 times C_m, respectively, corresponding to ρ/μ ratios of 0.29, 0.15, and 0.1, respectively.

VI. Conclusions

We propose an FSO multicast RNB switch architecture using T-SEs. In our design, signal splitting and switching are simultaneously performed within the same stage, and thus separate splitting stages, used in the conventional multicast switches, are not needed. The advantages of the switch proposed are twofold: first, there is a significant reduction in hardware complexity, as an $N \times N$ switch with full multicast capability requires *only* $N(N+1)/2$ *nonmovable* SEs; and second, a beam propagating in the switch proposed avoids the propagation loss that may be encountered by an optical beam passing through a splitting stage followed by a crossbar, as in SaD-based switches. This leads to lower insertion loss, which is due to the Gaussian beam divergence. Comparison with existing optical multicast switches shows that the proposed switch provides multicast capability with lower hardware complexity and a comparable performance. Cost analysis shows that for $N = 4$, the overall cost of the new design is lower than that of existing SNB switches, even if the T-SE is 4 to 10 times the cost of typical MEMS mirrors.

References

[1] International Data Corporation, 2015 [Online]. Available: https://www.idc.com/.

[2] A. Napoli, M. Bohn, D. Rafique, A. Stavdas, N. Sambo, L. Poti, M. Nolle, J. Fischer, E. Riccardi, A. Pagano, A. Di Giglio, M. Moreolo, J. Fabrega, E. Hugues-Salas, G. Zervas, D. Simeonidou, P. Layec, A. D'Errico, T. Rahman, and J. P. Gimenez, "Next generation elastic optical networks: The vision of the European research project IDEALIST," *IEEE Commun. Mag.*, vol. 53, no. 2, pp. 152–162, Feb. 2015.

[3] O. Liboiron-Ladouceur, I. Cerutti, P. G. Raponi, N. Andriolli, and P. Castoldi, "Energy-efficient design of a scalable optical multiplane interconnection architecture," *IEEE J. Sel. Top. Quantum Electron.*, vol. 17, no. 2, pp. 377–383, Mar. 2011.

[4] Y. Yin, R. Proietti, X. Ye, C. Nitta, V. Akella, and S. Yoo, "LIONS: An AWGR-based low-latency optical switch for high-performance computing and data centers," *IEEE J. Sel. Top. Quantum Electron.*, vol. 19, no. 2, 3600409, Mar. 2013.

[5] M. Imran, M. Collier, P. Landais, and K. Katrinis, "HOSA: Hybrid optical switch architecture for data center networks," in *ACM Int. Conf. on Computing Frontiers*, 2015, paper 27.

[6] S. Chua and B. Li, *Optical Switches: Materials and Design*, Woodhead Publishing Series in Electronic and Optical Materials. Elsevier Science, 2010.

[7] G. Baxter, S. Frisken, D. Abakoumov, H. Zhou, I. Clarke, A. Bartos, and S. Poole, "Highly programmable wavelength selective switch based on liquid crystal on silicon switching elements," in *Optical Fiber Communication Conf. and the Nat. Fiber Optic Engineers Conf. (OFC/NFOEC)*, 2006.

[8] H. S. Hamza, "On the design of multi-wavelength copy interconnects with reduced complexity," *Photon. Netw. Commun.*, vol. 19, no. 3, pp. 240–256, 2010.

[9] G. Shen, T. H. Cheng, S. K. Bose, C. Lu, and T. Y. Chai, "A novel rearrangeable non-blocking architecture for MEMS optical space switch," *Opt. Netw. Mag.*, vol. 3, no. 6, pp. 70–79, 2002.

[10] C. Li, G. Li, V. Li, P. Wai, H. Xie, and X. Yuan, "Using 2×2 switching modules to build large 2-D MEMS optical switches," in *IEEE Global Telecommunications Conf.*, 2003, pp. 2798–2802.

[11] W. Hu and Q. Zeng, "Multicasting optical cross connects employing splitter-and-delivery switch," *IEEE Photon. Technol. Lett.*, vol. 10, no. 7, pp. 970–972, 1998.

[12] C. Zhang and W. Hu, "Design and analysis of a multicast-capable optical cross-connect," *Proc. SPIE*, vol. 7136, 71364H, 2008.

[13] Y. Xin and G. Rouskas, "Multicast routing under optical layer constraints," in *Annu. Joint Conf. IEEE Computer and Communications Societies (INFOCOM)*, 2004, pp. 2731–2742.

[14] H. Du, W. Hu, H. He, C. Zhang, Y. Dong, W. Sun, W. Guo, Y. Jin, and S. Xiao, "Separated unicast/multicast splitter-and-delivery switch and its use in multicasting-capable optical cross-connect," *IEEE Photon. Technol. Lett.*, vol. 21, no. 6, pp. 368–370, 2009.

[15] A. S. Hamza, J. Deogun, and D. Alexander, "Free space optical multicast crossbar switch with non-movable switching elements," in *Advanced Photonics for Communications*, 2014, paper JT3A.13.

[16] A. S. Hamza, J. S. Deogun, and D. R. Alexander, "Free space optical multicast crossbar," *J. Opt. Commun. Netw.*, vol. 8, no. 1, pp. 1–10, Jan. 2016.

[17] A. S. Hamza, J. S. Deogun, and D. Alexander, "Rearrangeable non-blocking multicast FSO switch using fixed switching elements," in *IEEE Global Communications Conf.*, San Diego, California, 2015.

[18] R. A. Spanke and V. E. Benes, "N-stage planar optical permutation network," *Appl. Opt.*, vol. 26, no. 7, pp. 1226–1229, Apr. 1987.

[19] R. P. Stanley, *Enumerative Combinatorics: Volume 1*, 2nd ed., Cambridge Studies in Advanced Mathematics. New York, USA: Cambridge University, 2011.

[20] L. Y. Lin, E. Goldstein, and R. Tkach, "On the expandability of free-space micromachined optical cross connects," *J. Lightwave Technol.*, vol. 18, no. 4, pp. 482–489, 2000.

[21] K. Murata, T. Saida, K. Sano, I. Ogawa, H. Fukuyama, R. Kasahara, Y. Muramoto, H. Nosaka, S. Tsunashima, T. Mizuno, H. Tanobe, K. Hattori, T. Yoshimatsu, H. Kawakami, and E. Yoshida, "100-Gbit/s PDM-QPSK coherent receiver with wide dynamic range and excellent common-mode rejection ratio," *Opt. Express*, vol. 19, no. 26, pp. B125–B130, Dec. 2011.

[22] Kent Optronics, "Switchable mirror/switchable glass," 2012 [Online]. Available: http://kentoptronics.com/switchable.html.

[23] N. Hamedazimi, Z. Qazi, H. Gupta, V. Sekar, S. R. Das, J. P. Longtin, H. Shah, and A. Tanwer, "Firefly: A reconfigurable wireless data center fabric using free-space optics," in *ACM Special Interest Group on Data Communication (SIGCOMM)*, 2014, pp. 319–330.

[24] O. Solgaard, *Photonic Microsystems: Micro and Nanotechnology Applied to Optical Devices and Systems*. Springer, 2009.

[25] L. Y. Lin, E. L. Goldstein, and R. W. Tkach, "Free-space micromachined optical switches for optical networking," *IEEE J. Sel. Top. Quantum Electron.*, vol. 5, no. 1, pp. 4–9, 1999.

[26] V. Li, C. Y. Li, and P. K. A. Wai, "Alternative structures for two-dimensional MEMS optical switches [Invited]," *J. Opt. Netw.*, vol. 3, no. 10, pp. 742–757, Oct. 2004.